Design, Synthesis, and Preclinical Evaluation of New 5,6- (or 6,7-) Disubstituted-2-(fluorophenyl)quinolin-4-one Derivatives as Potent Antitumor Agents

ARTICLE *in* JOURNAL OF MEDICINAL CHEMISTRY · OCTOBER 2010

Impact Factor: 5.45 · DOI: 10.1021/jm100780c · Source: PubMed

Journal of Medicinal Chemistry Article

J. Med. Chem. **2010,** *53,* 8047–8058 **8047**
DOI: 10.1021/jm100780c

Design, Synthesis, and Preclinical Evaluation of New 5,6- (or 6,7-) Disubstituted-2-(fluorophenyl)quinolin-4-one Derivatives as Potent Antitumor Agents

Li-Chen Chou,[†,#] Meng-Tung Tsai,[†,#] Mei-Hua Hsu,[†] Sheng-Hung Wang,[‡] Tzong-Der Way,[§] Chi-Hung Huang,[∥] Hui-Yi Lin,[†] Keduo Qian,[⊥] Yizhou Dong,[⊥] Kuo-Hsiung Lee,[⊥] Li-Jiau Huang,*[,†] and Sheng-Chu Kuo*[,†]

[†]*Graduate Institute of Pharmaceutical Chemistry, China Medical University, Taichung, Taiwan,* [‡]*Institute of Cellular and Organismic Biology, Academia Sinica, 128 Academia Road, Section 2, Nankang, Taipei 115, Taiwan,* [§]*School of Biological Science and Technology, China Medical University, Taichung, Taiwan,* [∥]*Taiwan Advance Biopharm, Inc., 12F, No. 25, Lane 169, Kangning Street, Xizhi City, Taipei 221, Taiwan, and* [⊥]*Natural Products Research Laboratories, Eshelman School of Pharmacy, University of North Carolina, Chapel Hill, North Carolina 27599-7568, United States.* [#] *L.-C. Chou and M.-T. Tsai contributed equally to this work.*

Received June 24, 2010

Our previous exploration of 2-phenylquinolin-4-ones (2-PQs) has led to an anticancer drug candidate 2-(2-fluorophenyl)-6,7-methylenedioxyquinolin-4-one monosodium phosphate (CHM-1−P-Na). In order to develop additional new drug candidates, novel 2-PQs were designed, synthesized, and evaluated for cytotoxic activity. Most analogues, including **1b**, **2a**,**b**, **3a**,**b**, **4a**,**b**, and **5a**,**b**, exhibited significant inhibitory activity (IC_{50} of 0.03−8.2 μM) against all tested tumor cell lines. As one of the most potent analogue, 2-(3-fluorophenyl)-5-hydroxy-6-methoxyquinolin-4-one (**3b**) selectively inhibited 14 out of 60 cancer cell lines in a National Cancer Institute (NCI) evaluation. Preliminary mechanism of action study suggested that **3b** had a significant effect on the tyrosine autophosphorylation of insulin-like growth factor-1 receptor (IGF-1R). Safety pharmacology profiling of **3b** showed no significant effect on normal biological functions of most enzymes tested. Furthermore, sodium 2-(3-fluorophenyl)-6-methoxy-4-oxo-1,4-dihydroquinolin-5-yl phosphate (**15**), the monophosphate of **3b**, exceeded the activity of doxorubicin and was comparable to CHM-1−P-Na in a Hep3B xenograft nude mice model. In summary, **15** is a promising clinical candidate and is currently under preclinical study.

Introduction

During the past 2 decades, we have synthesized a series of substituted 2-phenylquinolin-4-ones (2-PQs[a])[1−4] (Figure 1) and identified them as a new class of anticancer agents. In a recent in vivo evaluation of a series of 2-PQs with potent cytotoxicity, excellent antitumor activity was identified with 2-(2-fluorphenyl)-6,7-methylenedioxyquinolin-4-one (CHM-1)[4] (Figure 1) and the sodium salt of its phosphate derivative 2-(2-fluorophenyl)-6,7-methylenedioxyquinolin-4-one monosodium phosphate (CHM-1−P-Na)[4,5] (Figure 1). Furthermore, both acute toxicity and safety pharmacology profiling (SPP) studies supported that CHM-1−P-Na is extremely safe to use. On the basis of the above findings, 2-PQ derivatives are a class of promising anticancer agents, which prompted us to design and develop additional new promising analogues as potential clinical trials candidates.

As mentioned above, CHM-1−P-Na exhibited excellent antitumor activity through both oral and iv administration. Its unique structure possesses three key functional groups. The first key moiety is a phosphate group located on the 4-position of its quinoline ring. As stated in our previous report,[4] a pharmacokinetic study of CHM-1−P-Na confirmed its rapid bioconversion into its active parent molecule CHM-1 following iv or po administration. It was also found that CHM-1−P-Na could be dephosphorylated by alkaline phosphatase into CHM-1 on the extracellular space of SKOV-3 tumor. Because alkaline phosphatase is known to be overexpressed on the extracellular space of specific tumor cells, such as ovarian and hepatic carcinoma cells, the introduction of a phosphate group appears to be a reasonable strategy for target delivery. Second, a methylenedioxy moiety bridges the 5- and 6-positions of the quinoline ring. This moiety could form an orthoquinone upon metabolism and subsequently be metabolized into more cytotoxic metabolites in hypoxic cells.[4,6] Because severe hypoxia is a common situation in locally advanced solid tumors, the incorporation of a methylenedioxy moiety becomes a meaningful antitumor approach. Third, a fluorine atom is located on the 2-phenyl group. In certain medicines, the unordinary nature of fluorine has been reported to impart a variety of properties, including enhanced potency, improved duration of action, and attenuation of biliary clearance.[7]

*To whom correspondence should be addressed. For L.-J.H.: phone, +886-4-22053366-5609; fax, +886-4-22030760; e-mail, ljhuang@mail.cmu.edu.tw. For S.-C.K.: phone, +886-4-22030760; fax, +886-4-22030760; e-mail, sckuo@mail.cmu.edu.tw.

[a] Abbreviations: 2-PQ, 2-phenylquinolin-4-one; SARs, structure−activity relationships; CHM-1, 2-(2-fluorophenyl)-6,7-methylenedioxyquinolin-4-one; CHM-1−P-Na, 2-(2-fluorophenyl)-6,7-methylenedioxyquinolin-4-one monosodium phosphate; SPP, safety pharmacology profiling; NCI, National Cancer Institute; GI_{50}, 50% growth inhibition; MG-MID, mean growth midpoint; TGI, total growth inhibition; 3-HP, 2-[(3-hydroxy-2-pyridinyl)methylene]hydrazinecarbothioamide; IGF-1R, insulin-like growth factor-1 receptor; PDB, Protein Data Bank; PQIP, *cis*-3-[3-(4-methylpiperazin-l-yl)cyclobutyl]-1-(2-phenylquinolin-7-yl)imidazo[1,5-*a*]pyrazin-8-ylamine; CYP450, cytochrome P450 enzymes; PDE, phosphodiesterase; YES1, V-yes-1 Yamaguchi sarcoma viral oncogene homologue 1; UGT1A1, UDP-glucuronosyltransferase 1A1; iv, intravenous; po, oral.

Published on Web 10/25/2010

Meanwhile, our prior structure−activity relationships (SARs)[1−3] have established that the presence of a group with a lone pair of electrons (for instance, OCH_3, NRR, Cl, F) at both the 6-position of the quinoline ring and 3′-position of the 2-phenyl group enhanced the cytotoxicity of 2-PQs. With this finding in mind, we have designed compounds **1**−**5** (Figure 2) and their related phosphates as our target compounds based on the following attributes: (1) the presence of an OR group at the quinoline 6-position, (2) the presence of a fluorine atom on the 2-phenyl group, and (3) ability to be metabolized into an orthoquinone in vivo.

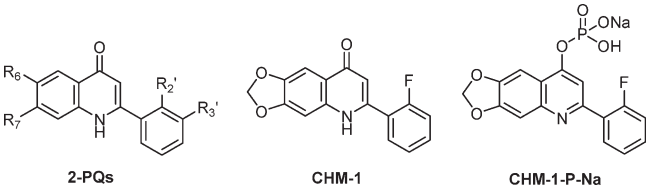

Figure 1. Structures of 2-PQs, CHM-1, and CHM-1−P-Na.

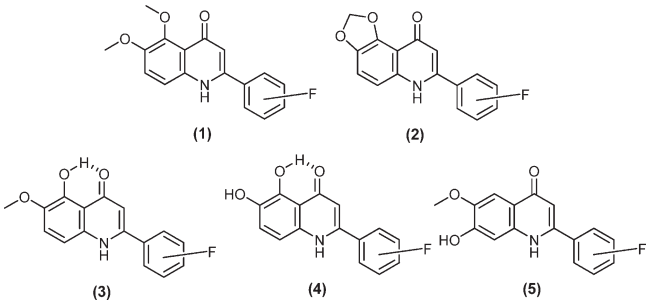

Figure 2. Structures of target compounds **1**−**5**.

Among the target compounds **1**−**5** synthesized and evaluated, analogue **3b** appeared to be the most potent cytotoxic agent. Further studies, including safety pharmacology profiling, mechanism of action, and molecular modeling of **3b**, as well as in vivo antitumor evaluation on its monophosphate **15**, were performed.

Chemistry

The synthetic route to 5,6,7,2′,3′,4′-substituted 2-phenylquinolin-4-ones (**1**, **2**, **6**) is illustrated in Scheme 1A. First, 3,4,5-substituted 1-amino-2-acetylbenzenes **7a**−**c** were reacted separately with 2,3,4-substituted benzoyl chlorides **8a**−**c** to yield the corresponding amides **9a**−**i**, which were subsequently cyclized in *t*-BuOH in the presence of *t*-BuOK to afford the target compounds (**1**, **2**, **6**). Starting materials 6-amino-2,3-dimethoxyacetophenone (**7a**),[8] 6-amino-2,3-methylenedioxyacetophenone (**7b**),[9] and 4-benzyloxy-3-methoxy-6-nitroacetophenone (**10**)[10] were prepared according to previously reported methods. As shown in Scheme 1B, nitro **10** was reduced by reaction with $SnCl_2$ to give 6-amino-3-methoxy-4-benzyloxyacetophenone (**7c**).

As shown in Scheme 2, selective demethylation of compounds **1a**−**c** with BCl_3 provided the corresponding 2-(fluorophenyl)-5-hydroxy-6-methoxyquinolin-4-ones **3a**−**c**, whose structures

Scheme 1

A

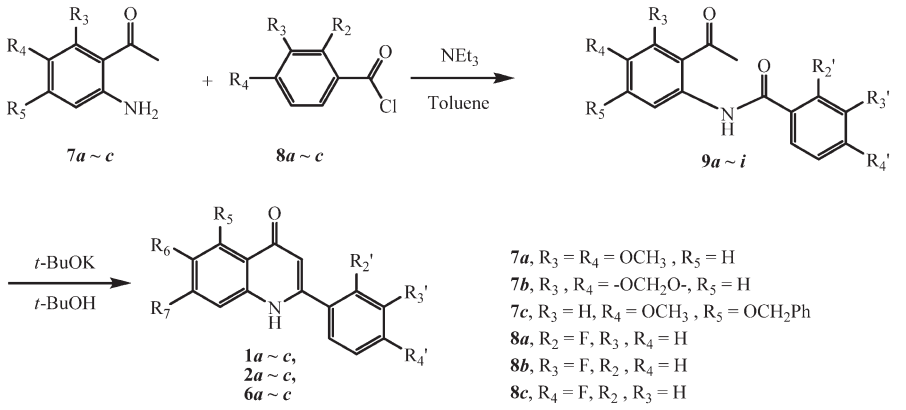

7*a*, $R_3 = R_4 = OCH_3$, $R_5 = H$
7*b*, R_3, $R_4 = -OCH_2O-$, $R_5 = H$
7*c*, $R_3 = H$, $R_4 = OCH_3$, $R_5 = OCH_2Ph$
8*a*, $R_2 = F$, R_3, $R_4 = H$
8*b*, $R_3 = F$, R_2, $R_4 = H$
8*c*, $R_4 = F$, R_2, $R_3 = H$

1*a*, $R_5 = R_6 = OCH_3$, $R_7 = H$, $R_2' = F$, R_3', $R_4' = H$
1*b*, $R_5 = R_6 = OCH_3$, $R_7 = H$, $R_3' = F$, R_2', $R_4' = H$
1*c*, $R_5 = R_6 = OCH_3$, $R_7 = H$, $R_4' = F$, R_2', $R_3' = H$
2*a*, R_5, $R_6 = -OCH_2O-$, $R_7 = H$, $R_2' = F$, R_3', $R_4' = H$
2*b*, R_5, $R_6 = -OCH_2O-$, $R_7 = H$, $R_3' = F$, R_2', $R_4' = H$
2*c*, R_5, $R_6 = -OCH_2O-$, $R_7 = H$, $R_4' = F$, R_2', $R_3' = H$
6*a*, $R_5 = H$, $R_6 = OCH_3$, $R_7 = OCH_2Ph$, $R_2' = F$, R_3', $R_4' = H$
6*b*, $R_5 = H$, $R_6 = OCH_3$, $R_7 = OCH_2Ph$, $R_3' = F$, R_2', $R_4' = H$
6*c*, $R_5 = H$, $R_6 = OCH_3$, $R_7 = OCH_2Ph$, $R_4' = F$, R_2', $R_3' = H$

9*a*, $R_3 = R_4 = OCH_3$, $R_5 = H$, $R_2' = F$, R_3', $R_4' = H$
9*b*, $R_3 = R_4 = OCH_3$, $R_5 = H$, $R_3' = F$, R_2', $R_4' = H$
9*c*, $R_3 = R_4 = OCH_3$, $R_5 = H$, $R_4' = F$, R_2', $R_3' = H$
9*d*, R_3, $R_4 = -OCH_2O-$, $R_5 = H$, $R_2' = F$, R_3', $R_4' = H$
9*e*, R_3, $R_4 = -OCH_2O-$, $R_5 = H$, $R_3' = F$, R_2', $R_4' = H$
9*f*, R_3, $R_4 = -OCH_2O-$, $R_5 = H$, $R_4' = F$, R_2', $R_3' = H$
9*g*, $R_3 = H$, $R_4 = OCH_3$, $R_5 = OCH_2Ph$, $R_2' = F$, R_3', $R_4' = H$
9*h*, $R_3 = H$, $R_4 = OCH_3$, $R_5 = OCH_2Ph$, $R_3' = F$, R_2', $R_4' = H$
9*i*, $R_3 = H$, $R_4 = OCH_3$, $R_5 = OCH_2Ph$, $R_4' = F$, R_2', $R_3' = H$

B

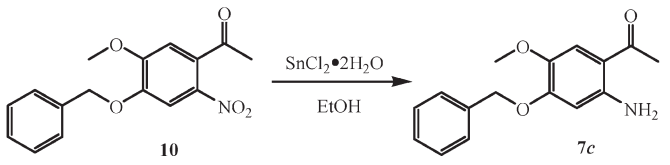

Scheme 2

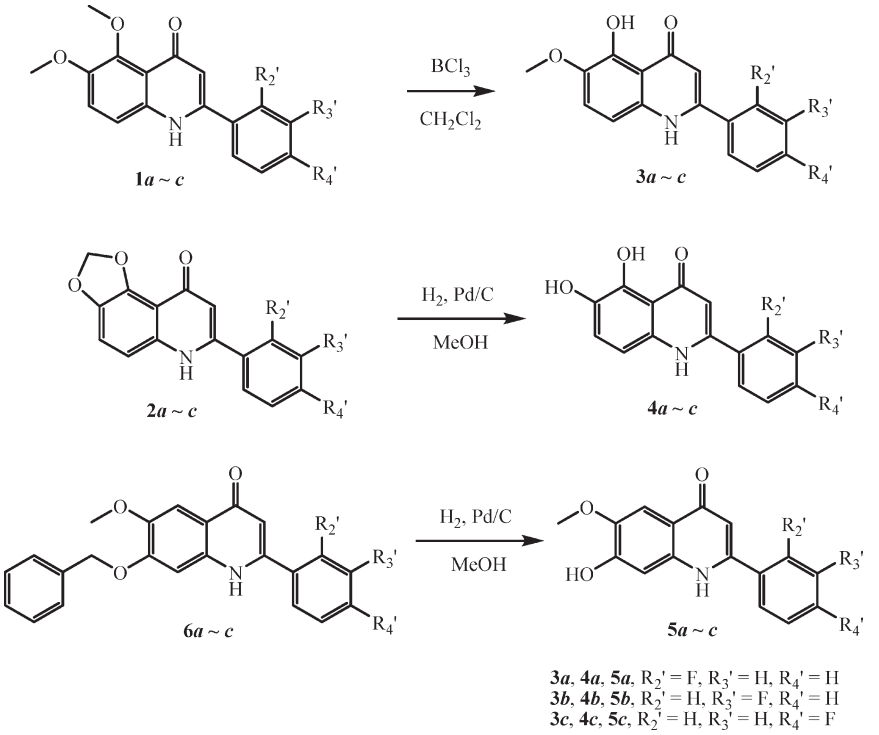

Scheme 3

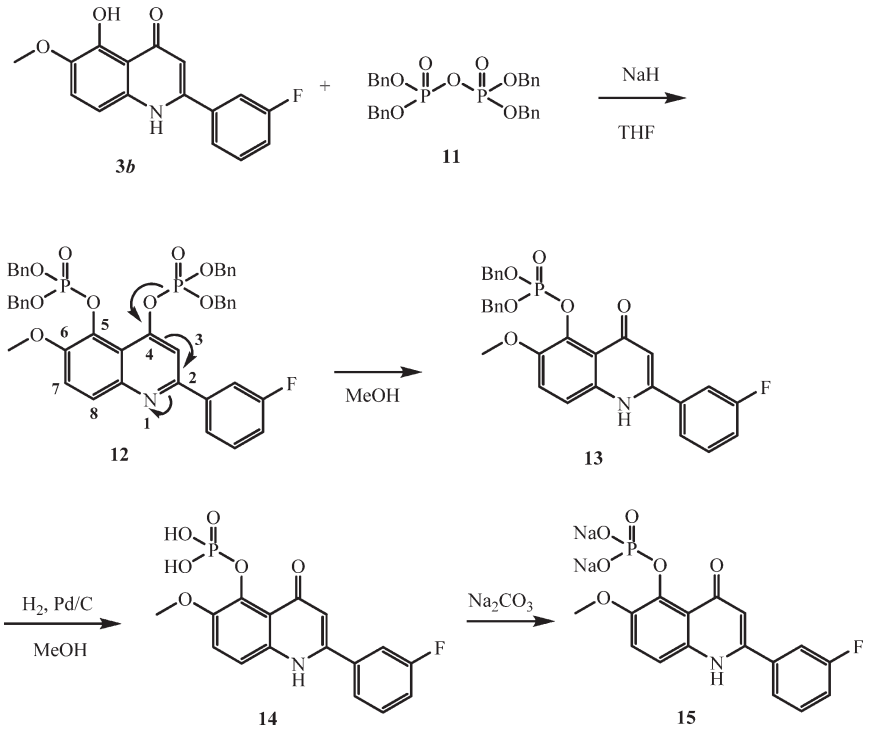

were confirmed by NOSY spectra. Catalytic hydrogenation of compounds **2a**−**c** and 7-benzyloxy-2-(fluorophenyl)-6-methoxyquinolin-4-ones **6a**−**c** yielded 2-(fluorophenyl)-5,6-dihydroxyquinolin-4-ones **4a**−**c** and 2-(fluorophenyl)-7-hydroxy-6-methoxyquinolin-4-ones **5a**−**c**, respectively.

The phosphorylation of 2-(3-fluorophenyl)-5-hydroxy-6-methoxyquinoline-4-one (**3b**) is shown in Scheme 3. Compound **3b** was first reacted with tetrabenzylpyrophosphate (**11**) in the presence of NaH to yield 2-(3-fluorophenyl)-6-methoxyquinoline-4,5-diyl bis(dibenzyl phosphate) (**12**) which was treated with MeOH at room temperature provided monophosphate **13**. Its structure was confirmed by the chemical shift of the proton on the 3-position (δ 6.27) in the ^{1}H NMR spectra. Monophosphoric acid **14** was obtained by catalytic hydrogenation of **13**. Finally, **14** was converted into water-soluble sodium salt **15**.

Table 1. Cytotoxicities of CHM-1 and Target Compounds **1**−**5**[a]

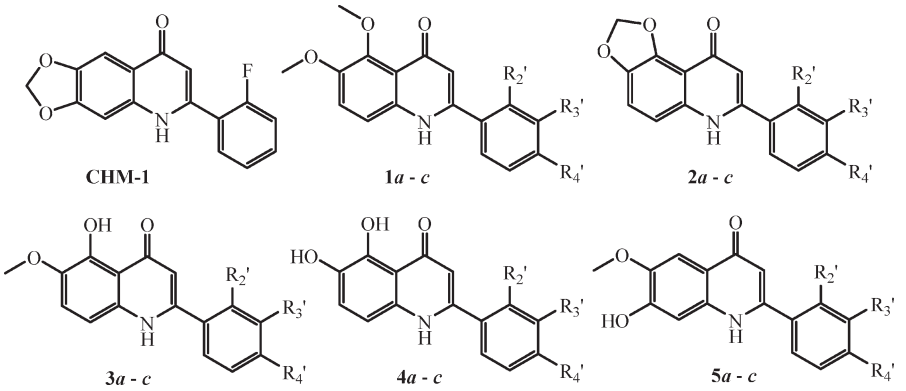

				IC_{50}[b] (μM)			
compd	R_2'	R_3'	R_4'	HL-60	HCT116	Hep3B	H460
CHM-1				0.08	0.15	0.13	0.14
1a	F	H	H	3.7	> 20	> 20	> 20
1b	H	F	H	1.3	1.2	2.6	3.5
1c	H	H	F	2.0	> 20	> 20	> 20
2a	F	H	H	1.0	2.1	1.9	4.5
2b	H	F	H	0.7	2.5	2.4	3.2
2c	H	H	F	> 10	> 10	> 10	> 10
3a	F	H	H	0.07	0.05	0.05	0.11
3b	H	F	H	0.03	0.07	0.07	0.08
3c	H	H	F	1.8	2.4	11.0	8.8
4a	F	H	H	0.5	0.6	3.9	4.1
4b	H	F	H	0.3	8.2	6.9	6.1
4c	H	H	F	38.6	> 100	100	100
5a	F	H	H	1.3	5.8	5.3	4.4
5b	H	F	H	0.9	1.1	5.3	4.8
5c	H	H	F	38.2	> 100	> 100	> 100

[a] Human tumor cells were treated with different concentrations of compounds for 48 h. [b] Data are presented as IC_{50} (μM, the concentration of 50% proliferation-inhibitory effect).

Results and Discussion

Growth Inhibitory Activity of 1−5 against Human Cancer Cell Lines. The 5,6- (6,7-) disubstituted 2-(fluorophenyl)-quinolin-4-ones **1**−**5** and CHM-1 were screened against HL-60, HCT-116, Hep3B, H-460 human tumor cell lines, and the results are summarized in Table 1. Among the 5,6-dimethoxy derivatives **1a**−**c**, the 3′-fluoro derivative **1b** exhibited the greatest cytotoxicity, although it was less potent than the positive control CHM-1. Meanwhile, both **2a** and **2b**, with a 5,6-methylenedioxy entity on the quinoline ring, demonstrated activity comparable to that of **1b**, although again they were less potent than CHM-1. While all three 5-hydroxy-6-methoxy derivatives **3a**−**c** showed significant cytotoxicity, compounds **3a** and **3b**, with the fluorine in the 2′ and 3′ positions, respectively, were better than **3c**, with the fluorine in the 4′ position. Changing the quinolone substitution pattern again from 5-hydroxy-6-methoxy (**3a**−**c**) to 5,6-dihydroxy (**4a**−**c**) or 7-hydroxy-6-methoxy (**5a**−**c**) led to decreased potency. However, similar rank orders of potency were found among all derivatives regarding the position of the fluoro substituent. Generally, 4′-fluorophenyl derivatives (**1c**−**5c**) were much less potent than the 2′-(**1a**−**5a**) and 3′-fluorophenyl (**1b**−**5b**) derivatives. In fact, only **1c** and **3c** showed significant activity against some tested cancer cell line. Overall, compounds **3a** and **3b** are considered the most promising anticancer agents, as they exhibited potent broad cytotoxic activity against all four cancer cell lines tested.

Compound **3b** was submitted for evaluation of activity against NCI's 60 human tumor cell line panel (Figure 3). The results demonstrated that **3b** was a potent antitumor agent against a broad range of human tumor cell lines [mean log GI_{50} (MG-MID) of −7.35]. As to total growth inhibition (TGI), **3b** also displayed potent inhibitory activity (TGI < 0.1 μM) against the following 14 cancer cell lines: HL-60, SR, NCI-H522, Colo 205, HCC-2998, HT-29, SF-539, SNB-75, MDA-MB-435, IGROV1, OVCAR-3, NCI/ADR-RES, RXF-393, and DU-145.

Unique COMPARE Fingerprint of 3b. The mean graph pattern (fingerprint) of **3b** was analyzed by a pattern-recognition computer program (COMPARE), which contains a database covering similar types of fingerprints from over 300 known anticancer agents with various mechanisms of action. The results of COMPARE analysis in Table 2 suggested that the mechanism of action of **3b** matched best with 2-[(3-hydroxy-2-pyridinyl)methylene]hydrazinecarbothioamide (3-HP). However, the low correlation coefficient (r < 0.558) implied that its mechanism of action was different from those of the anticancer agents covered in the COMPARE database.

Mechanism of Action of 3b. In our previous work,[4] we reported a multiple-targeting action mechanism for CHM-1. More recently,[11] we found that CHM-1 also affected the insulin-like growth factor-1 receptor (IGF-1R), which is gaining recognition as an attractive anticancer treatment target.[12] Because IGF-1R is frequently overexpressed in a

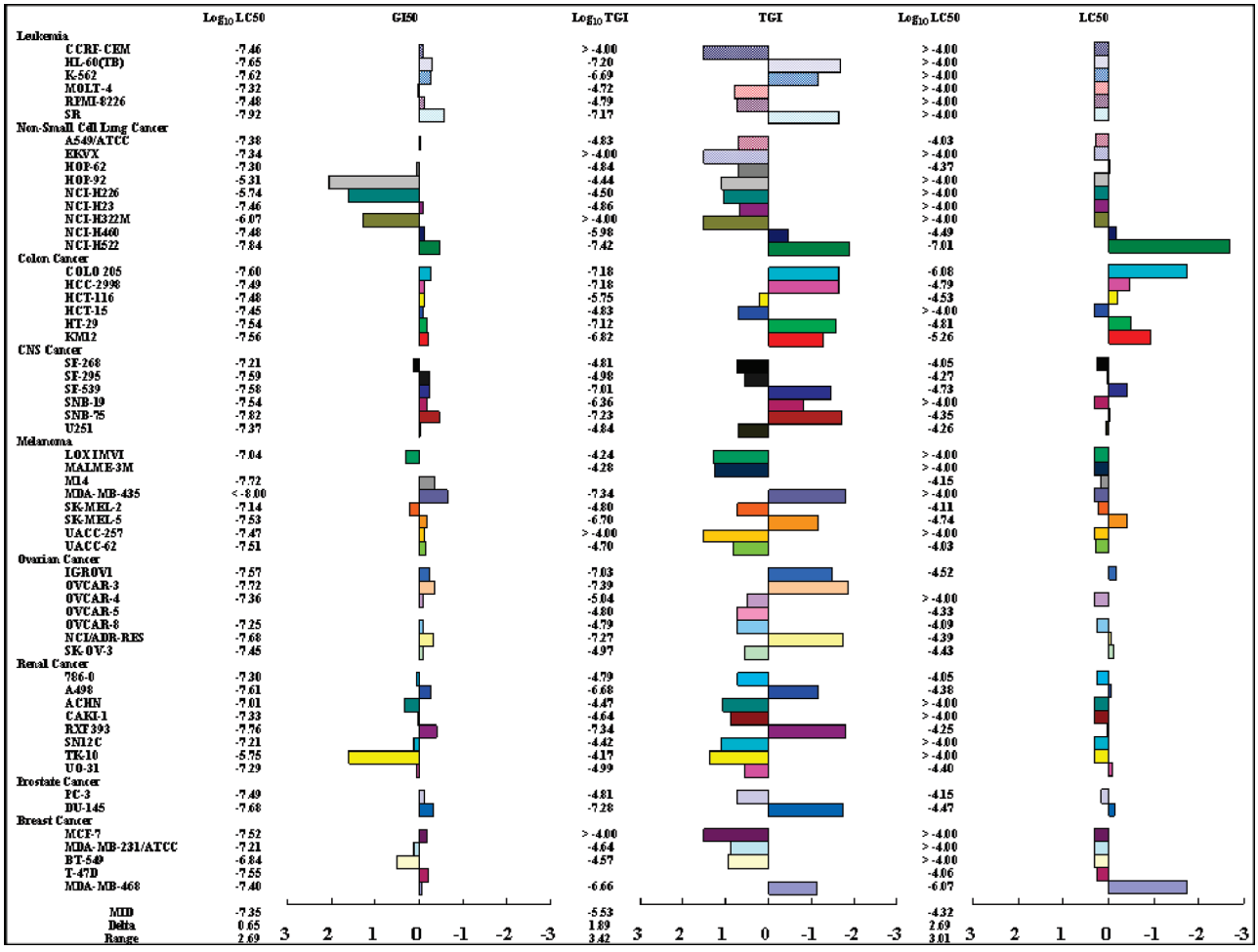

Figure 3. Differential activity patterns for compound **3b** against 60 human cancer cell lines. MG-MID: mean of log X values (X = GI_{50}, TGI, and LC_{50}). Delta: logarithm of the difference between the MG-MID and the log X of the most sensitive cell line. Range: logarithm of the difference between the log X of the most resistant cell line and the log X of the most sensitive cell line.

Table 2. Results of COMPARE cCorrelation at GI_{50} Level for Compound **3b**

rank	compound (NCI number)	r [a]	mechanism of action category
1	3HP[b] (NSC 95678)	0.558	DNA antimetabolite
2	trimetrexate (NSC 352122)	0.416	RNA/DNA antimetabolite
3	methotrexate (NSC 740)	0.395	RNA/DNA antimetabolite
4	rhizoxin (NSC 332598)	0.383	antimitotic agent
5	maytansine (NSC 153858)	0.379	antimitotic agent
6	thalicarpine (NSC 68075)	0.366	inhibits the synthesis of DNA, RNA, and protein
7	pancratiastatin (NSC 349156)	0.359	inhibition of the cell cycle from G0/G1 to S phase
8	paclitaxel (NSC 125973)	0.351	antimitotic agent
9	DUP 785[c] (NSC 368390)	0.348	RNA/DNA antimetabolite
10	5-fluorouracil (NSC 19893)	0.34	RNA/DNA antimetabolite

[a] r: correlation coefficient. [b] 3HP: 2-[(3-hydroxy-2-pyridinyl)methylene]hydrazinecarbothioamide. [c] DUP 785: brequinar sodium [6-fluoro-2-(2′-fluoro-1,1′-biphenyl-4-yl)-3-methyl-4-quinolinecarboxylic acid sodium salt].

number of human tumors and is considered an important anticancer target,[13,14] we investigated the effect of **3b** on IGF-1R expression in Hep3B cells, by examining receptor phosphorylation by the IGF-1R tyrosine kinase, in the presence or absence of **3b**. As shown in Figure 4, the cells were treated with different doses of **3b** for 12 h with DMSO as a control. Western blot analysis of IGF-1R phosphorylation with the antibody against PY1135/1136-IGF-1R showed that the concentration of phosphor-IGF-1R decreased gradually with increasing concentration of **3b**. The expression of IGF-1R, as evaluated by antibody to its β-subunit, served as loading control. The preliminary result indicated that **3b** had a significant effect on the tyrosine autophosphorylation of IGF-1R.

To delineate the interaction between **3b** and IGF-1R kinase, structural models of Protein Data Bank (PDB) entries 1K3A[15] and 3D94[16] were selected for molecular modeling study. PDB 1K3A is a complex structure of human IGF-1R kinase, which illustrates the ATP and Tyr-peptide substrate binding sites. On the other hand, PDB entry 3D94 illustrates the binding mode of the ATP-competitive inhibitor *cis*-3-[3-(4-methylpiperazin-l-yl)cyclobutyl]-1-(2-phenylquinolin-7-yl)imidazo[1,5-*a*]pyrazin-8-ylamine (PQIP), which

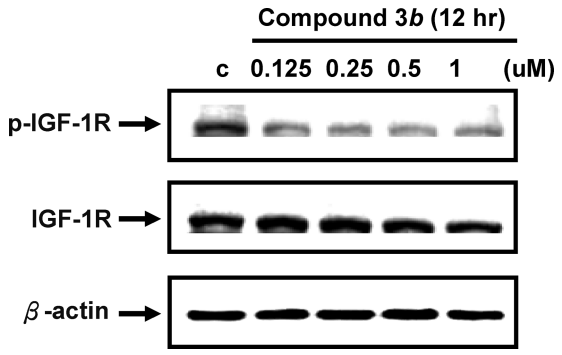

Figure 4. Effect of **3b** on basal receptor tyrosine phosphorylation (pTyr) in Hep3B cells. Hep3B cells were treated with various concentrations of **3b** at 37 °C for 12 h. Levels of phosphorylated IGF-1R and IGF-1R were analyzed by immunoblotting. Immunoblotting with β-actin antibody demonstrated equivalent protein in each lane. Western blot data presented are representative of those obtained in at least three separate experiments.

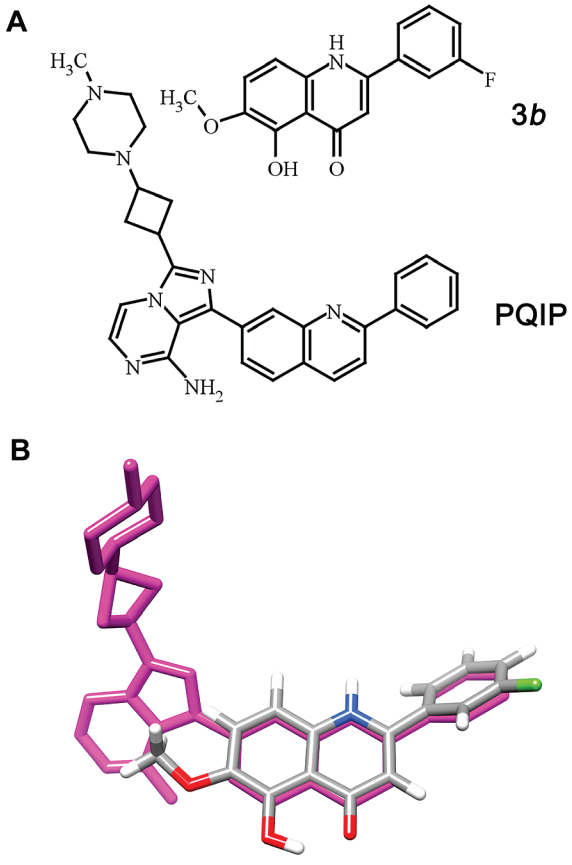

Figure 5. (A) Chemical structure of compound **3b** and PQIP. (B) Structural similarity between **3b** and PQIP. PQIP possesses a 2-phenylquinolinyl segment, which is superimposable with **3b**.

contains a 2-phenylquinolinyl segment that can be superimposed on compound **3b** because of structural similarity (Figure 5).

During molecular modeling, the structural features of IGF-1R kinase with different ligand-bound states were first compared through molecular 3D superimposition. As shown in Figure 6, the conformation of the activation loop changed dramatically between ATP-bound (model 1K3A, yellow color) and PQIP-bound (model 3D94, magenta color) states. The autophosphorylation of Tyr-1131, Tyr-1135, and Tyr-1136 on the activation loop is also inhibited by PQIP.

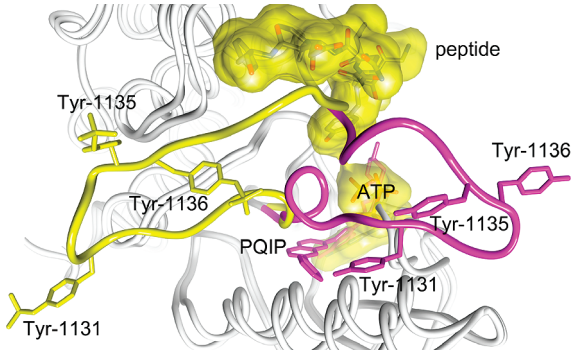

Figure 6. Structural superimposition of IGF1R model 1K3A and 3D94. The structural features of IGF1R kinase were compared between ATP-bound (1K3A, yellow color) and PQIP-bound (3D94, magenta color) states. At the PQIP-bound state, the conformation of the activation loop containing Tyr-1131, Tyr-1135, and Tyr-1136 changed dramatically, compared with ATP-bound state.

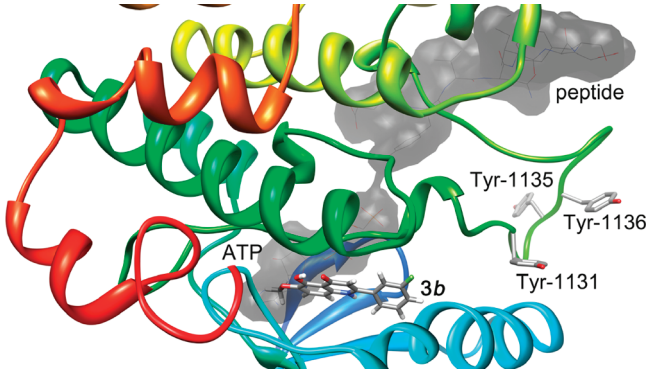

Figure 7. Predicted binding mode of compound **3b** with IGF1R kinase. Binding site of **3b** is the same as that of 2-phenylquinolinyl segment of PQIP, which is beside the ATP-binding site. The binding sites of ATP and peptide substrate are indicated as shaded regions according to model 1K3A.

The binding pocket of PQIP was then used for predicting the interaction mode of compound **3b** against IGF-1R kinase. Molecular docking study showed that **3b** interacted with IGF-1R directly at the binding site of the 2-phenylquinolinyl segment of PQIP (Figure 7). The results indicate that the comparable binding is due to structural similarity.

On the basis of the molecular modeling study described above, the structure of PQIP consists of two segments. One is an ATP-superimposable scaffold, and the other is a **3b**-superimposable scaffold (Figure 8). Furthermore, the **3b**-binding site can be identified as a potential allosteric binding site, which is unique and different from the ATP-binding site. Thus, **3b** might inhibit autophosphorylation of the activation loop by changing its conformation, without significantly interfering with ATP-binding. Therefore, this model could explain why the autophosphorylation of IGF-1R was inhibited by compound **3b**. The exact action mechanism of **3b** will be explored further.

Safety Pharmacology Profiling (SPP) of 3b. To explore its general pharmacological activities, **3b** was tested in 158 types of enzyme spectrum screening assays (Table 3). At 10 μM, **3b** inhibited the activity of only the following five enzymes: cytochrome P450 enzymes (CYP450), phosphodiesterase 4 (PDE4), phosphodiesterase 5 (PED5), V-yes-1 Yamaguchi sarcoma viral oncogene homologue 1 (YES1),

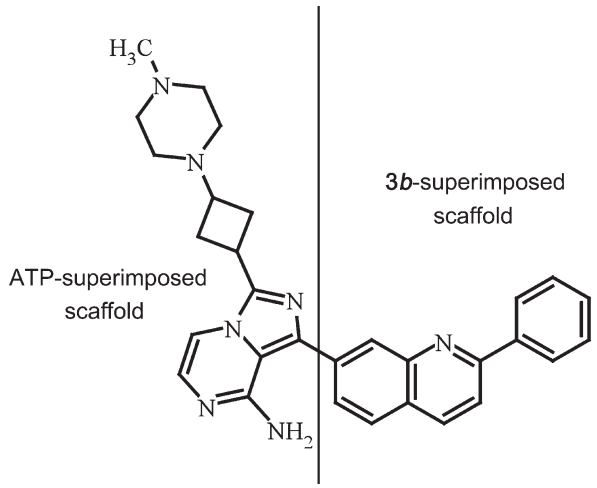

Figure 8. Structure of PQIP can be identified as two segments, including ATP-superimposed scaffold and **3b**-superimposed scaffold. Thus, **3b** is probably an allosteric inhibitor, which might inhibit autophosphorylation of activation loop without interfering with ATP-binding.

Table 3. Inhibitory Effects of **3b** on Enzyme Spectrum Screen Assays for SPP[a]

primary biochemical assay	species	concn (μM)	inhibtion (%)
CYP450, 1A2	hum	10	85
phosphodiesterase, PDE4	hum	10	55
phosphodiesterase, PDE5	hum	10	57
protein tyrosine kinase, YES1	hum	10	68
UDP-glucuronosyltransferase, UGT1A1	hum	10	86

[a] hum = human. A standard error of the mean is presented where results are based on multiple, independent determinations.

and UDP-glucuronosyltransferase 1A1 (UGT1A1). Its inhibitory activity was most profound against UGT1A1. Interestingly, a recent study by E. Selga identified UGT1A1 as an important gene code in methotrexate resistance.[17] The author speculated that UGT1A1 may be associated with the drug resistance of certain cancer cell lines. The above results indicated that the SPP of **3b** differed from that of CHM-1.

In Vivo Antitumor Activity of 15. The water-soluble monophosphate of **3b** (**15**) was evaluated in the Hep3B xenograft nude mice model by oral route (po) at doses of 7.5, 15, and 30 (mg/kg)/day. As shown in Figure 9A−C, **15** induced dose- and time-dependent inhibition of Hep3B tumor growth. Significant tumor growth suppression, at an extent exceeding that observed after 10 (mg/kg)/day oral dosing of doxorubicin, was detected after 7.5 (mg/kg)/day oral dosing of **15**. Nearly complete tumor suppression was observed after 30 (mg/kg)/day oral dosing. During the course of antitumor evaluation, no significant body weight changes were detected in either the tested or the control mice. Similarly, the dose- and time-dependent antitumor test results by iv administration, summarized in Figure 9D−F, resembled those obtained by oral administration and generally indicated slightly better antitumor activity. Overall, the antitumor activity of **15** administrated po or iv is comparable with that of CHM-1−P-Na.

Conclusion

Novel 2-PQ analogues (**1**−**5**) were designed, synthesized, and evaluated for antitumor activity. Preliminary SAR of the new analogues was established. As one of our most promising target compounds, **3b** was submitted for evaluation of activity against NCI's 60 human tumor cell line panel.[18,19] The NCI results confirmed that compound **3b** had potent inhibitory activity against 14 cancer cell lines. The preliminary result of a mechanistic study indicated that **3b** had a significant effect on the tyrosine autophosphorylation of IGF-1R, which is an attractive target for anticancer therapy. The SPP results from enzyme assays suggested that **3b** has a clear-cut pharmacological effect on tumor-associated UGT1A1. Furthermore, a second target compound, **15**, the monophosphate derivative of **3b**, demonstrated excellent antitumor activity in nude mice bearing Hep3B xenograft, when administrated via po and iv routes. Excitingly, the antitumor activity of **15** exceeded that of doxorubicin, the most common drug used in current practice, and **15** was comparable to CHM-1−P-Na. In summary, **15** is a promising antitumor agent, which merits further exploration as a clinical candidate.

Experimental Section

Chemistry. General Experimental Procedures. All reagents and solvents were obtained commercially and used without further purification. Reactions were monitored by thin-layer chromatography (TLC), using Merck plates with fluorescent indicator (TLC silica gel 60 F_{254}). The following adsorbent was used for column chromatography: silica gel 60 (Merck, particle size 0.063−0.200 mm). Melting points were determined on a Yanaco MP-500D melting point apparatus and are uncorrected. IR spectra were recorded on Shimadzu IR Prestige-21 spectrophotometers as KBr pellets. NMR spectra were obtained on a Bruker Avance DPX-200 FT NMR spectrometer in $CDCl_3$ or DMSO. The following abbreviations are used: s, singlet; d, doublet; t, triplet; q, quartet; dd, double doublet; m, multiplet. EI mass spectra were measured with an HP 5995 GC−MS instrument. ESI mass spectra were measured with a Finnigan LCQ ion-trap mass spectrometer (TSQ Quantum, Thermo Finnigan Corporation, San Jose, CA). Elemental analyses (C, H, and N) were performed on a Perkin-Elmer 2400 series II CHNS/O analyzer, and the results were within ±0.4% of the calculated values. The purity of tested compounds was ≥95% as determined by HPLC conducted on a Shimadzu LC-10AT apparatus equipped with a Shimadzu SPD-M10AVP diode array detector and a Shimadzu SIL-10A autoinjector.

***N*-(2-Acetyl-3,4-dimethoxyphenyl)-2-fluorobenzamide (9a).** To a solution of 2-fluorobenzoyl chloride (**8a**, 0.48 g, 2.46 mmol) in 40 mL of dry toluene were added triethylamine (0.5 mL) and compound **7a**[8] (0.70 g, 4.43 mmol). The mixture was stirred at 55−60 °C for 30 min and then poured into crushed ice and extracted with EtOAc. The organic layer was washed with brine, dried over $MgSO_4$, and evaporated. The crude product was purified by column chromatography (silica gel, EtOAc/*n*-hexane) to give **9a** (0.5 g, 1.58 mmol) as a yellow solid. Yield: 64.1%. Mp 106−108 °C. MS (EI, 70 eV): *m*/*z* 317 (M^+). ^{1}H NMR (DMSO-d_6, 200 MHz): δ 2.45 (s, 3H), 3.76 (s, 3H), 3.81 (s, 3H), 7.14 (d, J = 2.6 Hz, 2H), 7.24−7.34 (m, 2H), 7.52−7.63 (m, 2H), 10.07 (s, 1H). ^{13}C NMR (DMSO-d_6, 50 MHz): δ 31.91, 56.52, 61.42, 114.52, 116.70, 121.43, 124.16, 125.06, 126.81, 130.52, 131.50, 133.35 (d, J = 8.0 Hz), 145.98, 150.47, 159.61 (d, J = 247.5 Hz), 163.19, 201.38. Anal. ($C_{17}H_{16}FNO_4$) C, H, N.

***N*-(2-Acetyl-3,4-dimethoxyphenyl)-3-fluorobenzamide (9b). 9b** was obtained from **7a** and 3-fluorobenzoyl chloride (**8b**). Yellow solid. Yield: 65.0%. Mp 98−99 °C. MS (EI, 70 eV): *m*/*z* 317 (M^+). ^{1}H NMR (DMSO-d_6, 200 MHz): δ 2.43 (s, 3H), 3.76 (s, 3H), 3.81 (s, 3H), 7.03−7.15 (m, 2H), 7.39−7.71 (m, 4H), 10.18 (s, 1H). ^{13}C NMR (DMSO-d_6, 50 MHz): δ 31.74, 56.45, 61.38, 114.30, 114.73 (d, J = 23 Hz), 119.04 (d, J = 21 Hz), 121.98, 124.13, 126.91, 131.12 (d, J = 7.5 Hz), 132.27, 136.89 (d, J = 6.5 Hz),

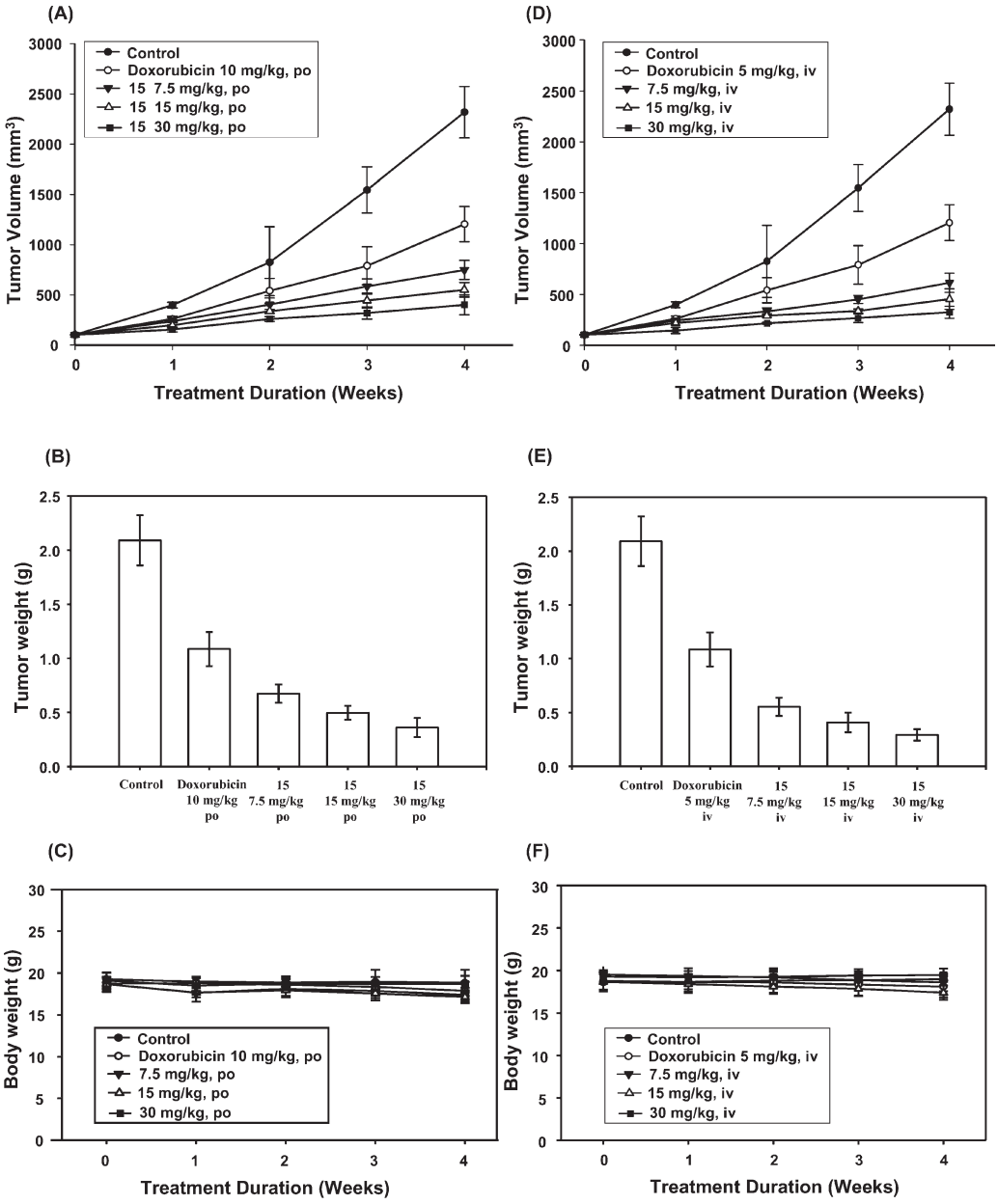

Figure 9. (A) Mean tumor volume−time profiles, (B) mean tumor weight−time profiles, and (C) mean body weight−time profiles in Hep3B xenograft nude mice (n = 11) following po dosing of doxorubicin at 10 mg/kg and **15** at 7.5, 15, and 30 mg/kg 5 days per week for 4 consecutive weeks. (D) Mean tumor volume−time profiles, (E) mean tumor weight−time profiles (F), and mean body weight−time profiles in Hep3B xenograft nude mice (n = 11) following iv dosing of doxorubicin at 5 mg/kg and **15** at 7.5, 15, and 30 mg/kg 5 days per week for 4 consecutive weeks.

145.90, 150.65, 162.40 (d, J = 243 Hz), 164.67, 201.22. Anal. ($C_{17}H_{16}FNO_4$) C, H, N.

***N*-(2-Acetyl-3,4-dimethoxyphenyl)-4-fluorobenzamide (9c). 9c** was obtained from **7a** and 4-fluorobenzoyl chloride (**8c**). Yellow solid. Yield: 64.7%. Mp 146−147 °C. MS (EI, 70 eV): m/z 317 (M^+). ^{1}H NMR (DMSO-d_6, 200 MHz): δ 2.43 (s, 3H), 3.76 (s, 3H), 3.81 (s, 3H), 7.03−7.14 (m, 2H), 7.26−7.35 (m, 2H), 7.88−7.95 (m, 2H), 10.14 (s, 1H). ^{13}C NMR (DMSO-d_6, 50 MHz): δ 31.76, 56.48, 61.38, 114.33, 115.83 (d, J = 22 Hz), 121.91, 127.17, 130.65 (d, J = 9.0 Hz), 131.06, 132.21, 145.90, 150.53, 164.57 (d, J = 247 Hz), 164.94, 201.25. Anal. ($C_{17}H_{16}FNO_4$) C, H, N.

***N*-(2-Acetyl-3,4-methylenedioxyphenyl)-2-fluorobenzamide (9d). 9d** was obtained from **7b**[9] and **8a**. Yellow solid. Yield: 90.0%. Mp 165−166 °C. MS (EI, 70 eV): m/z 301 (M^+). ^{1}H NMR (DMSO-d_6, 200 MHz): δ 2.53 (s, 3H), 6.13 (s, 2H), 7.12 (d, J = 8.6 Hz, 1H), 7.28−7.38 (m, 2H), 7.56−7.61 (m, 1H), 7.72−7.82 (m, 1H), 7.85 (d, J = 8.8 Hz, 1H), 11.50 (s, 1H). ^{13}C NMR (DMSO-d_6, 50 MHz): δ 32.53, 102.57, 111.92, 112.52, 114.74, 116.94 (d, J = 22.5 Hz), 123.55 (d, J = 12.5 Hz), 125.41, 130.98, 131.91, 134.04 (d, J = 8.5 Hz), 144.46, 149.00, 157.18, 162.22, 199.61. Anal. ($C_{16}H_{12}FNO_4$) C, H, N.

***N*-(2-Acetyl-3,4-methylenedioxyphenyl)-3-fluorobenzamide (9e). 9e** was obtained from **7b** and **8b**. Yellow solid. Yield: 95.0%. Mp 170−171 °C. MS (EI, 70 eV): m/z 301 (M^+). ^{1}H NMR (DMSO-d_6, 200 MHz): δ 2.56 (s, 3H), 6.14 (s, 2H), 7.13 (d, J = 8.4 Hz, 1H), 7.43 (t, J = 8.6 Hz, 1H), 7.52−7.68 (m, 2H), 7.72 (d, J = 8.6 Hz, 2H), 11.56 (s, 1H). ^{13}C NMR (DMSO-d_6, 50 MHz): δ 32.48, 102.61, 112.48, 112.62, 114.48 (d, J = 23 Hz), 114.89, 119.30 (d, J = 21.5 Hz), 123.56, 131.52 (d, J = 8.0 Hz), 131.96, 137.32, 144.61, 148.88, 162.61 (d, J = 243.5 Hz), 163.97, 199.88. Anal. ($C_{16}H_{12}FNO_4$) C, H, N.

***N*-(2-Acetyl-3,4-methylenedioxyphenyl)-4-fluorobenzamide (9f). 9f** was obtained from **7b** and **8c**. Yellow solid. Yield: 84.0%.

Mp 185−186 °C. MS (EI, 70 eV): *m*/*z* 301 (M^+). ^{1}H NMR (DMSO-d_6, 200 MHz): δ 2.51 (s, 3H), 6.13 (s, 2H), 7.12 (d, *J* = 8.6 Hz, 1H), 7.20−7.40 (m, 2H), 7.77 (d, *J* = 8.6 Hz, 1H), 7.89−7.97 (m, 2H), 11.58 (s, 1H). ^{13}C NMR (DMSO-d_6, 50 MHz): δ 32.55, 102.55, 111.20, 112.61, 114.54, 116.26 (d, *J* = 22 Hz), 130.22 (d, *J* = 7.0 Hz), 131.47, 132.41, 144.36, 148.97, 162.22, 164.67 (d, *J* = 248 Hz), 200.04. Anal. ($C_{16}H_{12}FNO_4$) C, H, N.

2-Amino-4-benzyloxy-5-methoxyacetophenone (7c). To a solution of **10**[10] (1.0 g, 3.32 mmol) in anhydrous EtOH (100 mL) was added $SnCl_2 \cdot 2H_2O$ (3.7 g, 16.4 mmol). The mixture was refluxed for 2 h and then cooled to 25 °C and poured in 5% $NaHCO_3$ solution. The precipitate was collected and washed with H_2O and then extracted with EtOAc. The extract was washed with H_2O, dried over $MgSO_4$, and evaporated. The crude product was purified by column chromatography (SiO_2, *n*-hexane/EtOAc = 1:1) to give **7c**. Yellow solid. Yield: 72.2%. Mp 135−137 °C. ^{1}H NMR (DMSO-d_6, 200 MHz): δ 2.39 (s, 3H), 3.66 (s, 3H), 5.03 (s, 2H), 6.38 (s,1H), 7.05 (s, 2H), 7.10 (s, 1H), 7.30−7.50 (m, 5H). ^{13}C NMR (DMSO-d_6, 50 MHz): δ 28.21, 56.94, 69.87, 100.05, 109.70, 115.40, 128.34, 128.49, 128.93, 136.83, 139.45, 148.74, 154.64, 198.06. Anal. ($C_{16}H_{17}NO_3$) C, H, N.

***N*-(2-Acetyl-5-benzyloxy-4-methoxyphenyl)-2-fluorobenzamide (9g). 9g** was obtained from **7c** and **8a**. Yellow solid. Yield: 89.0%. Mp 142−143 °C. MS (EI, 70 eV): *m*/*z* 393 (M^+). ^{1}H NMR (DMSO-d_6, 200 MHz): δ 2.60 (s, 3H), 3.82 (s, 3H), 5.16 (s, 2H), 7.10−7.50 (m, 8H), 7.56−7.67 (m, 1H), 7.80−7.89 (m, 1H), 8.57 (s, 1H), 12.45 (d, *J* = 4.0 Hz,1H). ^{13}C NMR (DMSO-d_6, 50 MHz): δ 29.08, 56.42, 70.41, 105.31, 115.28, 116.05, 117.08 (d, *J* = 22 Hz), 123.27 (d, *J* = 12.5 Hz), 125.60, 128.58, 128.95, 131.20, 134.45 (d, *J* = 8.5 Hz), 135.77, 136.50, 144.46, 152.98, 157.26, 162.35, 201.78. Anal. ($C_{23}H_{20}FNO_4$) C, H, N.

***N*-(2-Acetyl-5-benzyloxy-4-methoxyphenyl)-3-fluorobenzamide (9h). 9h** was obtained from **7c** and **8b**. Yellow solid. Yield: 86.6%. Mp 162−163 °C. MS (EI, 70 eV): *m*/*z* 393 (M^+). ^{1}H NMR (DMSO-d_6, 200 MHz): δ 2.62 (s, 3H), 3.81 (s, 3H), 5.15 (s, 2H), 7.26−7.52 (m, 7H), 7.54−7.78 (m, 3H), 8.51 (s, 1H), 12.70 (s, 1H). ^{13}C NMR (DMSO-d_6, 50 MHz): δ 29.10, 56.42, 70.40, 104.74, 114.45, 115.29, 115.83, 119.59 (d, *J* = 21.5 Hz), 123.36, 128.53, 128.95, 131.74 (d, *J* = 7.5 Hz), 136.28, 136.45, 137.30 (d, *J* = 6.5 Hz), 144.43, 153.26, 162.71 (d, *J* = 244 Hz), 163.91, 202.48. Anal. ($C_{23}H_{20}FNO_4$) C, H, N.

***N*-(2-Acetyl-5-benzyloxy-4-methoxyphenyl)-4-fluorobenzamide (9i). 9i** was obtained from **7c** and **8c**. Yellow solid. Yield: 67.1%. Mp 168−169 °C. MS (EI, 70 eV): *m*/*z* 393 (M^+). ^{1}H NMR (DMSO-d_6, 200 MHz): δ 2.63 (s, 3H), 3.81 (s, 3H), 5.15 (s, 2H), 7.2−7.5 (m, 7H), 7.9−8.1 (m, 3H), 8.54 (s, 1H), 12.69 (s, 1H). ^{13}C NMR (DMSO-d_6, 50 MHz): δ 29.11, 56.47, 70.41, 104.73, 115.39, 115.83, 116.27, 116.72, 128.53, 128.94, 130.17 (d, *J* = 9.0 Hz), 132.54 (d, *J* = 9.5 Hz), 136.48, 136.58, 144.33, 153.33, 164.24, 166.82, 202.48. Anal. ($C_{23}H_{20}FNO_4$) C, H, N.

2-(2-Fluorophenyl)-5,6-dimethoxyquinolin-4-one (1a). To a suspension of **9a** (0.50 g, 1.58 mmol) in *tert*-butyl alcohol (30 mL) was added potassium *tert*-butoxide (1.0 g, 8.93 mmol). The mixture was refluxed under argon for 20 h and evaporated. The residue was treated with a 10% NH_4Cl solution (30 mL). The solid precipitate was collected and washed with *n*-hexane and Me_2CO. The crude product was recrystallized from MeOH to afford **1a** as yellow needles (0.27 g, 0.9 mmol). Yield: 57.1%. Mp 215−217 °C. MS (EI, 70 eV): *m*/*z* 299 (M^+). IR (KBr): 1628 (C=O) cm^{-1}. ^{1}H NMR (DMSO-d_6, 200 MHz): δ 3.72 (s, 3H), 3.81 (s, 3H), 6.06 (s, 1H), 7.3−7.6 (m, 5H), 7.60−7.71 (m, 1H). Anal. ($C_{17}H_{14}FNO_3$) C, H, N. HPLC purity analysis. Column: Thermo ODS Hypersil, 150 mm × 4.6 mm, 5 μm. Mobile phase: 0.01 M sodium hydrogen carbonate/acetonitrile = 30/70. Detection wavelength: PDA Ch1 254 nm at 4 nm. Retention time: 1.999 min. Flow rate: 1.0 mL/min. Purity: 98.35%.

2-(3-Fluorophenyl)-5,6-dimethoxyquinolin-4-one (1b). 1b was obtained from **9b**. Yellow needles. Yield: 53.1%. Mp 190−192 °C. MS (EI, 70 eV): *m*/*z* 299 (M^+). IR (KBr): 1599 (C=O) cm^{-1}. ^{1}H NMR (DMSO-d_6, 200 MHz): δ 3.73 (s, 3H), 3.81 (s, 3H), 6.35 (s, 1H), 7.28−7.40 (m, 1H), 7.46−7.60 (m, 3H), 7.64−7.76 (m, 2H). Anal. ($C_{17}H_{14}FNO_3$) C, H, N. HPLC purity analysis. Column: Thermo ODS Hypersil, 150 mm × 4.6 mm, 5 μm. Mobile phase: 0.01 M sodium hydrogen carbonate/acetonitrile = 30/70. Detection wavelength: PDA Ch1 254 nm at 4 nm. Retention time: 2.067 min. Flow rate: 1.0 mL/min. Purity: 98.54%.

2-(4-Fluorophenyl)-5,6-dimethoxyquinolin-4-one (1c). 1c was obtained from **9c**. White needles. Yield: 54.6%. Mp 227−229 °C. MS (EI, 70 eV): *m*/*z* 299 (M^+). IR (KBr): 1607 (C=O) cm^{-1}. ^{1}H NMR (DMSO-d_6, 200 MHz): δ 3.72 (s, 3H), 3.80 (s, 3H), 6.26 (s, 1H), 7.31−7.40 (m, 2H), 7.44−7.54 (m, 2H), 7.83−7.90 (m, 2H). Anal. ($C_{17}H_{14}FNO_3$) C, H, N. HPLC purity analysis. Column: Thermo ODS Hypersil, 150 mm × 4.6 mm, 5 μm. Mobile phase: 0.01 M sodium hydrogen carbonate/acetonitrile = 30/70. Detection wavelength: PDA Ch1 254 nm at 4 nm. Retention time: 2.054 min. Flow rate: 1.0 mL/min. Purity: 98.86%.

2-(2-Fluorophenyl)-5,6-methylenedioxyquinolin-4-one (2a). 2a was obtained from **9d**. Yellow solid. Yield: 47.6%. Mp 282−283 °C. MS (EI, 70 eV): *m*/*z* 283 (M^+). IR (KBr): 1605 (C=O) cm^{-1}. ^{1}H NMR (DMSO-d_6, 200 MHz): δ 5.92 (s, 1H), 6.11 (s, 2H), 7.09 (d, *J* = 8.8 Hz, 1H), 7.27−7.38 (m, 3H), 7.55−7.70 (m, 2H), 11.71 (s, 1H). Anal. ($C_{16}H_{10}FNO_3$) C, H, N. HPLC purity analysis. Column: Thermo ODS Hypersil, 150 mm × 4.6 mm, 5 μm. Mobile phase: methanol/0.05% TFA in water = 75/25. Detection wavelength: PDA Ch1 254 nm at 4 nm. Retention time: 2.377 min. Flow rate: 1.0 mL/min. Purity: 99.16%.

2-(3-Fluorophenyl)-5,6-methylenedioxyquinolin-4-one (2b). 2b was obtained from **9e**. White solid. Yield: 44.9%. Mp 286−288 °C. MS (EI, 70 eV): *m*/*z* 283 (M^+). IR (KBr): 1609 (C=O) cm^{-1}. ^{1}H NMR (DMSO-d_6, 200 MHz): δ 6.11 (s, 2H), 6.19 (s, 1H), 7.19−7.36 (m, 3H), 7.55−7.67 (m, 3H), 11.71 (s, 1H). Anal. ($C_{16}H_{10}FNO_3$) C, H, N. HPLC purity analysis. Column: Thermo ODS Hypersil, 150 mm × 4.6 mm, 5 μm. Mobile phase: methanol/0.05% TFA in water = 75/25. Detection wavelength: PDA Ch1 254 nm at 4 nm. Retention time: 2.516 min. Flow rate: 1.0 mL/min. Purity: 98.63%.

2-(4-Fluorophenyl)-5,6-methylenedioxyquinolin-4-one (2c). 2c was obtained from **9f**. White solid. Yield: 45.9%. Mp 286−288 °C. MS (EI, 70 eV): *m*/*z* 283 (M^+). IR (KBr): 1613 (C=O) cm^{-1}. ^{1}H NMR (DMSO-d_6, 200 MHz): δ 6.10 (s, 3H), 7.17−7.31 (m, 2H), 7.32−7.41 (m, 2H), 7.78−7.85 (m, 2H), 11.46 (s, 1H). Anal. ($C_{16}H_{10}FNO_3$) C, H, N. HPLC purity analysis. Column: Thermo ODS Hypersil, 150 mm × 4.6 mm, 5 μm. Mobile phase: methanol/0.05% TFA in water = 75/25. Detection wavelength: PDA Ch1 254 nm at 4 nm. Retention time: 2.500 min. Flow rate: 1.0 mL/min. Purity: 97.93%.

7-Benzyloxy-2-(2-fluorophenyl)-6-methoxyquinolin-4-one (6a). 6a was obtained from **9g**. White solid. Yield: 60.5%. Mp 132−134 °C. MS (EI, 70 eV): *m*/*z* 375 (M^+). ^{1}H NMR (DMSO-d_6, 200 MHz): δ 3.82 (s, 3H), 5.16 (s, 2H), 6.21 (s, 1H), 7.20−7.80 (m, 11H). ^{13}C NMR (DMSO-d_6, 50 MHz): δ 56.02, 70.40, 101.86, 104.14, 108.80, 116.77 (d, *J* = 21.5 Hz), 118.86, 123.30 (d, *J* = 13 Hz), 125.43, 128.50, 128.97, 131.24, 132.56 (d, *J* = 8.0 Hz), 136.58, 137.08, 144.73, 147.73, 152.52, 159.64 (d, *J* = 247 Hz), 174.57. Anal. ($C_{23}H_{18}FNO_3$) C, H, N.

7-Benzyloxy-2-(3-fluorophenyl)-6-methoxyquinolin-4-one (6b). 6b was obtained from **9h**. White solid. Yield: 64.3%. Mp 154−155 °C. MS (EI, 70 eV): *m*/*z* 375 (M^+). ^{1}H NMR (DMSO-d_6, 200 MHz): δ 3.83 (s, 3H), 5.17 (s, 2H), 6.56 (s, 1H), 7.30−7.50 (m, 8H), 7.55−7.60 (m, 1H), 7.60−7.80 (m, 2H). ^{13}C NMR (DMSO-d_6, 50 MHz): δ 56.07, 70.45, 102.27, 103.72, 106.03, 114.71 (d, *J* = 23.5 Hz), 117.56 (d, *J* = 20.5 Hz), 118.44, 123.95, 128.56, 128.99, 131.50, 136.49, 137.41, 148.02, 148.44, 152.72, 165.13, 173.61. Anal. ($C_{23}H_{18}FNO_3$) C, H, N.

7-Benzyloxy-2-(4-fluorophenyl)-6-methoxyquinolin-4-one (6c). 6c was obtained from **9i**. White solid. Yield: 64.4%. Mp 248−249 °C. MS (EI, 70 eV): *m*/*z* 375 (M^+). ^{1}H NMR (DMSO-d_6,

200 MHz): δ 3.80 (s, 3H), 5.13 (s, 2H), 6.26 (s, 1H), 7.20−7.60 (m, 9H), 7.80−8.00 (m, 2H). ^{13}C NMR (DMSO-d_6, 50 MHz): δ 55.96, 70.36, 101.41, 104.51, 106.61, 116.30 (d, J = 21.5 Hz), 119.27, 128.56, 128.99, 130.05 (d, J = 8.0 Hz), 136.60, 147.39, 148.06, 152.19, 163.63 (d, J = 246.5 Hz), 176.10. Anal. ($C_{23}H_{18}FNO_3$) C, H, N.

2-(2-Fluorophenyl)-5-hydroxy-6-methoxyquinolin-4-one (3a). To a solution of **1a** (0.2 g, 0.67 mmol) in CH_2Cl_2 (3 mL) was added 5 mL of BCl_3 solution (1 M in CH_2Cl_2) dropwise at 0 ± 1 °C. The mixture was stirred at 25 ± 1 °C for 2 h and then poured into crushed ice and extracted with EtOAc. The organic layer was washed with H_2O, dried over $MgSO_4$, and evaporated. The crude was purified by column chromatography (SiO_2, $CHCl_3$/MeOH = 15:1) and recrystallized from MeOH to give **3a**. Yellow solid. Yield: 24.1%. Mp 268−270 °C. MS (EI, 70 eV): m/z 285 (M^+). IR (KBr): 1604.77 (C=O) cm^{-1}. ^{1}H NMR (DMSO-d_6, 200 MHz): δ 3.78 (s, 3H), 6.11 (s, 1H), 7.01 (d, J = 7.4 Hz,1H), 7.36−7.48 (m, 3H), 7.54−7.72 (m, 2H), 12.25 (s, 1H), 14.54 (s, 1H). ^{13}C NMR (DMSO-d_6, 50 MHz): δ 55.80, 106.22, 106.43, 112.88, 116.36 (d, J = 23 Hz), 120.81, 121.96 (d, J = 13.5 Hz), 125.04, 130.85, 132.67 (d, J = 8.6 Hz), 135.09, 141.02, 146.27, 149.29, 158.92 (d, J = 247.7 Hz), 181.97. Anal. ($C_{16}H_{12}FNO_3$) C, H, N. HPLC purity analysis. Column: Thermo ODS Hypersil, 150 mm × 4.6 mm, 5 μm. Mobile phase: 0.01 M sodium hydrogen carbonate/acetone = 30/70. Detection wavelength: PDA Ch1 254 nm at 4 nm. Retention time: 1.954 min. Flow rate: 1.0 mL/min. Purity: 96.04%.

2-(3-Fluorophenyl)-5-hydroxy-6-methoxyquinolin-4-one (3b). **3b** was obtained from **1b** and BCl_3. Yellow solid. Yield: 26.7%. Mp 274−276 °C. MS (EI, 70 eV): m/z 285 (M^+). IR (KBr): 1606.70 (C=O) cm^{-1}. ^{1}H NMR (DMSO-d_6, 200 MHz): δ 3.77 (s, 3H), 6.33 (s, 1H), 7.11 (d, J = 8.8 Hz,1H), 7.33−7.48 (m, 2H), 7.51−7.76 (m, 3H), 12.09 (s, 1H), 14.56 (s, 1H). ^{13}C NMR (DMSO-d_6, 50 MHz): δ 57.19, 104.82, 106.97, 113.39, 115.09 (d, J = 23 Hz), 118.06 (d, J = 21 Hz), 121.07, 124.32, 131.64 (d, J = 9.0 Hz), 135.61, 136.16 (d, J = 8.0 Hz), 141.49, 149.64, 150.12, 162.64 (d, J = 242.5 Hz), 182.69. Anal. ($C_{16}H_{12}FNO_3$) C, H, N. HPLC purity analysis. Column: Thermo ODS Hypersil, 150 mm × 4.6 mm, 5 μm. Mobile phase: 0.01 M sodium hydrogen carbonate/acetonitrile = 30/70. Detection wavelength: PDA Ch1 254 nm at 4 nm. Retention time: 1.820 min. Flow rate: 1.0 mL/min. Purity: 99.13%.

2-(4-Fluorophenyl)-5-hydroxy-6-methoxyquinolin-4-one (3c). **3c** was obtained from **1c** and BCl_3. Yellow solid. Yield: 23.0%. Mp 307−309 °C. MS (EI, 70 eV): m/z 285 (M^+). IR (KBr): 1610.56 (C=O) cm^{-1}. ^{1}H NMR (DMSO-d_6, 200 MHz): δ 3.76 (s, 3H), 6.25 (s, 1H), 7.08 (d, J = 9.0 Hz, 1H), 7.34−7.43 (m, 3H), 7.82−7.89 (m, 2H), 12.01 (s, 1H), 14.60 (s, 1H). ^{13}C NMR (DMSO-d_6, 50 MHz): δ 57.19, 104.53, 106.84, 113.23, 116.47 (d, J = 22 Hz), 120.99, 130.55 (d, J = 9.0 Hz), 135.62, 141.45, 149.69, 150.64, 164.02 (d, J = 247 Hz), 182.59. Anal. ($C_{16}H_{12}FNO_3$) C, H, N. HPLC purity analysis. Column: Thermo ODS Hypersil, 150 mm × 4.6 mm, 5 μm. Mobile phase: 0.01 M sodium hydrogen carbonate/acetonitrile = 30/70. Detection wavelength: PDA Ch1 254 nm at 4 nm. Retention time: 1.822 min. Flow rate: 1.0 mL/min. Purity: 98.00%.

2-(2-Fluorophenyl)-5,6-dihydroxyquinolin-4-one (4a). A solution of **2a** (0.1 g, 0.35 mmol) in anhydrous MeOH (30 mL) was hydrogenated in the presence of 10% Pd/C (0.2 g) at 25 ± 2 °C for 40 h. The catalyst was filtered off, and the filtrate was evaporated. The crude was purified by column chromatography (SiO_2, EtOAc/MeOH = 30:1) to give **4a**. White solid. Yield: 13.7%. Mp 152−154 °C. MS (EI, 70 eV): m/z 271 (M^+). IR (KBr): 1622.13 (C=O) cm^{-1}. ^{1}H NMR (DMSO-d_6, 200 MHz): δ 6.03 (s, 1H), 7.15 (d, J = 8.8 Hz,1H), 7.30−7.70 (m, 6H), 9.72 (s, 1H), 11.76 (s, 1H). ^{13}C NMR (DMSO-d_6, 50 MHz): δ 107.67, 108.57, 116.75 (d, J = 21.5 Hz), 120.54, 122.67, 123.36, 125.42, 126.70, 131.22, 132.49, 134.35, 144.30, 154.29, 159.43 (d, J = 248.5 Hz), 176.82. Anal. ($C_{15}H_{10}FNO_3$) C, H, N. HPLC purity analysis. Column: Thermo ODS Hypersil, 150 mm × 4.6 mm, 5 μm. Mobile phase: methanol/0.05% TFA in water = 75/25. Detection wavelength: PDA Ch1 254 nm at 4 nm. Retention time: 2.384 min. Flow rate: 1.0 mL/min. Purity: 96.50%.

2-(3-Fluorophenyl)-5,6-dihydroxyquinolin-4-one (4b). **4b** was obtained from **2b**. White solid. Yield: 15.0%. Mp 307−308 °C. MS (EI, 70 eV): m/z 271 (M^+). IR (KBr): 1608.63 (C=O) cm^{-1}. ^{1}H NMR (DMSO-d_6, 200 MHz): δ 6.25 (s, 1H), 7.15 (d, J = 8.8 Hz, 1H), 7.30−7.50 (m, 2H), 7.50−7.80 (m, 4H), 9.72 (s, 1H), 11.60 (s, 1H). ^{13}C NMR (DMSO-d_6, 50 MHz): δ 106.38, 107.57, 114.65 (d, J = 23 Hz), 117.38 (d, J = 21.5 Hz), 120.91, 122.62, 123.91, 126.81, 131.52 (d, J = 8.5 Hz), 134.45, 137.17, 147.66, 154.36, 162.70 (d, J = 242 Hz), 176.82. Anal. ($C_{15}H_{10}FNO_3$) C, H, N. HPLC purity analysis. Column: Thermo ODS Hypersil, 150 mm × 4.6 mm, 5 μm. Mobile phase: methanol/0.05% TFA in water = 75/25. Detection wavelength: PDA Ch1 254 nm at 4 nm. Retention time: 2.485 min. Flow rate: 1.0 mL/min. Purity: 99.51%.

2-(4-Fluorophenyl)-5,6-dihydroxyquinolin-4-one (4c). **4c** was obtained from **2c**. White solid. Yield: 13.9%. Mp 332−334 °C. MS (EI, 70 eV): m/z 271 (M^+). IR (KBr): 1614.42 (C=O) cm^{-1}. ^{1}H NMR (DMSO-d_6, 200 MHz): δ 6.18 (s, 1H), 7.14 (dd, J = 9.0, 2.8 Hz, 1H), 7.33−7.42 (m, 3H), 7.59 (d, J = 8.8 Hz, 1H), 7.79−7.86 (m, 2H), 9.70 (s, 1H), 11.59 (s, 1H). ^{13}C NMR (DMSO-d_6, 50 MHz): δ 106.24, 107.68, 116.39 (d, J = 21.5 Hz), 120.71, 122.48, 126.73, 130.19 (d, J = 8.5 Hz), 131.38, 134.42, 148.24, 154.20, 163.70 (d, J = 247.5 Hz), 176.81. Anal. ($C_{15}H_{10}FNO_3$) C, H, N. HPLC purity analysis. Column: Thermo ODS Hypersil, 150 mm × 4.6 mm, 5 μm. Mobile phase: methanol/0.05% TFA in water = 75/25. Detection wavelength: PDA Ch1 254 nm at 4 nm. Retention time: 2.502 min. Flow rate: 1.0 mL/min. Purity: 99.40%.

2-(2-Fluorophenyl)-7-hydroxy-6-methoxyquinolin-4-one (5a). Compound **6a** (0.3 g, 0.80 mmol) was allowed to react in the same manner as described in the preparation of compound **4a** to give **5a**. White solid. Yield: 61.3%. Mp 277−279 °C. MS (EI, 70 eV): m/z 285 (M^+). IR (KBr): 1622.13 (C=O) cm^{-1}. ^{1}H NMR (DMSO-d_6, 200 MHz): δ 3.82 (s, 3H), 6.04 (s, 1H), 7.01 (s, 1H), 7.32−7.50 (m, 3H), 7.50−7.67 (m, 2H), 10.22 (s, 1H), 11.68 (s, 1H). ^{13}C NMR (DMSO-d_6, 50 MHz): δ 55.52, 102.72, 105.37, 108.20, 116.28 (d, J = 22.5 Hz), 118.07, 122.94, 124.92, 130.75, 131.99 (d, J = 7.95 Hz), 136.45, 143.61, 146.58, 151.59, 158.98 (d, J = 246.9 Hz), 175.30. Anal. ($C_{16}H_{12}FNO_3$) C, H, N. HPLC purity analysis. Column: Thermo ODS Hypersil, 150 mm × 4.6 mm, 5 μm. Mobile phase: methanol/0.05% TFA in water = 75/25. Detection wavelength: PDA Ch1 254 nm at 4 nm. Retention time: 2.667 min. Flow rate: 1.0 mL/min. Purity: 99.39%.

2-(3-Fluorophenyl)-7-hydroxy-6-methoxyquinolin-4-one (5b). **5b** was obtained from **6b**. White solid. Yield: 44.8%. Mp 326−328 °C. MS (EI, 70 eV): m/z 285 (M^+). IR (KBr): 1606.70 (C=O) cm^{-1}. ^{1}H NMR (DMSO-d_6, 200 MHz): δ 3.81 (s, 3H), 6.24 (s, 1H), 7.12 (s, 1H), 7.27−7.42 (m, 2H), 7.47−7.70 (m, 3H), 10.20 (s, 1H), 11.44 (s, 1H). ^{13}C NMR (DMSO-d_6, 50 MHz): δ 55.92, 103.35, 104.70, 106.67, 114.59 (d, J = 23 Hz), 117.26 (d, J = 21 Hz), 118.85, 123.85, 131.47 (d, J = 8.0 Hz), 136.85, 137.16, 146.94, 147.33, 151.93, 162.69 (d, J = 242.5 Hz), 176.37. Anal. ($C_{16}H_{12}FNO_3$) C, H, N. HPLC purity analysis. Column: Thermo ODS Hypersil, 150 mm × 4.6 mm, 5 μm. Mobile phase: methanol/0.05% TFA in water = 75/25. Detection wavelength: PDA Ch1 254 nm at 4 nm. Retention time: 2.754 min. Flow rate: 1.0 mL/min. Purity: 99.38%.

2-(4-Fluorophenyl)-7-hydroxy-6-methoxyquinolin-4-one (5c). **5c** was obtained from **6c**. White solid. Yield: 42.5%. Mp 352−354 °C. MS (EI, 70 eV): m/z 285 (M^+). IR (KBr): 1610.56 (C=O) cm^{-1}. ^{1}H NMR (DMSO-d_6, 200 MHz): δ 3.80 (s, 3H), 6.19 (s, 1H), 7.11 (s, 1H), 7.20−7.50 (m, 3H), 7.70−7.90 (m, 2H). ^{13}C NMR (DMSO-d_6, 50 MHz): δ 55.89, 103.50, 104.55, 106.18, 116.30 (d, J = 21.5 Hz), 118.41, 130.03 (d, J = 8.5 Hz), 131.57, 137.22, 147.00, 148.01, 152.21, 163.58 (d, J = 246 Hz), 175.93. Anal. ($C_{16}H_{12}FNO_3$) C, H, N. HPLC purity analysis. Column: Thermo ODS Hypersil, 150 mm × 4.6 mm,

5 μm. Mobile phase: methanol/0.05% TFA in water = 75/25. Detection wavelength: PDA Ch1 254 nm at 4 nm. Retention time: 2.736 min. Flow rate: 1.0 mL/min. Purity: 99.40%.

2-(3-Fluorophenyl)-6-methoxyquinoline-4,5-diyl Bis(dibenzyl phosphate) (12). To a stirred solution of **3b** (0.12 g, 0.42 mmol) in dry THF (20 mL) was added NaH (96 mg, 4 mmol) at 0 ± 1 °C. After the mixture was stirred for 1 h, tetrabenzyl pyrophosphate (**11**) (430 mg, 0.8 mmol) was added and stirring was continued for 25 min. The reaction mixture was filtered and washed with CH_2Cl_2. The filtrate was concentrated under vacuum at a temperature below 30 °C. The residue was purified by column chromatography (SiO_2, *n*-hexane/EtOAc) to give **12**. Liquid. Yield: 95.0%. MS (EI, 70 eV): *m*/*z* 805 (M^+). ^{1}H NMR (DMSO-d_6, 200 MHz): δ 3.87 (s, 3H), 5.10 (s, 2H), 5.14 (s, 2H), 5.18 (s, 2H), 5.22 (s, 2H), 7.20−7.36 (m, 21H), 7.47−7.60 (m, 1H), 7.72−7.84 (m, 4H), 8.01 (d, *J* = 9.4 Hz, 1H). ^{13}C NMR (DMSO-d_6, 50 MHz): δ 57.27, 69.63, 69.74, 70.12, 70.23, 110.20, 113.57, 114.03, 116.23, 116.92, 117.35, 119.48, 123.28, 128.10, 128.38, 128.70, 128.79, 128.85, 128.95, 131.35, 131.51, 135.79, 135.94, 136.32, 136.47, 140.41, 140.56, 145.39, 149.74, 149.82, 153.44, 153.57, 153.92, 160.71, 165.56. Anal. ($C_{44}H_{38}FNO_9P_2$) C, H, N.

Dibenzyl 2-(3-Fluorophenyl)-6-methoxy-4-oxo-1,4-dihydroquinolin-5-yl phosphate (13). A suspension of **12** (2.42 g, 3.0 mmol) in anhydrous MeOH (10 mL) was stirred at 25 °C for 24 h. The precipitates were collected and purified by column chromatography (SiO_2, *n*-hexane/EtOAc) to give **13**. Yellow solid. Yield: 80.0%. Mp 136−138 °C. MS (ESI): *m*/*z* 544.5 $(M - H)^-$. ^{1}H NMR (DMSO-d_6, 200 MHz): δ 3.75 (s, 3H), 5.28 (s, 2H), 5.31 (s, 2H), 6.27 (s, 1H), 7.26−7.50 (m, 11H), 7.50−7.78 (m, 6H). ^{13}C NMR (DMSO-d_6, 50 MHz): δ 57.19, 69.32, 69.44, 108.51, 114.46, 114.93, 116.74, 117.38, 119.24, 123.92, 128.04, 128.51, 128.82, 131.49, 131.65, 136.74, 137.07, 137.23, 147.00, 160.29, 176.88. Anal. ($C_{30}H_{25}FNO_6P$) C, H, N.

2-(3-Fluorophenyl)-6-methoxy-4-oxo-1,4-dihydroquinolin-5-yl Dihydrogen Phosphate (14). A suspension of **13** (250 mg, 0.46 mmol) in anhydrous MeOH (10 mL) was hydrogenated in the presence of 10% Pd/C (125 mg) at 25 °C for 15 min. The catalyst and precipitate were collected and dissolved in 10% $NaHCO_3$ solution and then filtered. The filtrate was acidified with dilute HCl and the precipitate was then collected and washed with acetone to give **14**. Yellow solid. Yield: 63.7%. Mp 179−181 °C. MS(ESI): *m*/*z* 366 $(M + H)^+$. ^{1}H NMR (D_2O + NaOD, 200 MHz): δ 3.76 (s, 3H), 6.53 (s, 1H), 7.05 (*t*, *J* = 8.4 Hz, 1H), 7.24−7.60 (m, 5H). Anal. ($C_{16}H_{13}FNO_6P$) C, H, N.

Sodium 2-(3-Fluorophenyl)-6-methoxy-4-oxo-1,4-dihydroquinolin-5-yl Phosphate (15). To a stirred solution of $NaHCO_3$ (0.34 g, 4.0 mmol) in H_2O (20 mL) was added **14** (0.73 g, 2.0 mmol) at 0 ± 1 °C. After the addition was complete, the reaction mixture was removed from the ice bath, stirred at 25 °C for 10 min, and then filtered though Celite, after no dissolution from the solid was observed. The resulting filtrate (15 mL) was poured into acetone (60 mL) and kept in an ice bath for 1 h. The precipitate was collected and washed with ice-cooled acetone (10 mL × 5). The solid was dried under vacuum to give **15**. Yellow solid. Yield: 48.0%. Mp > 300 °C. MS(ESI): *m*/*z* 410 $(M + H)^+$. ^{1}H NMR (D_2O, 200 MHz): δ 3.72 (s, 3H), 6.54 (s, 3H), 6.99 (*t*, *J* = 7.8 Hz, 1H), 7.15−7.55 (m, 5H). Anal. ($C_{16}H_{11}FNNa_2O_6P$) C, H, N.

Biological Assays. MTT (3-(4,5-Dimethylthiazol-2-yl)-2,5-diphenyltetrazolium Bromide) Assays.[20,21] HL-60, HCT-116, Hep 3B, and H460 cells were treated with tested compounds for the indicated periods. After treatment, cells were washed once with PBS and incubated with MTT (Sigma, St. Louis, MO) for 2 h. The formazan precipitate was dissolved in 150 μL of DMSO, and the absorbance was measured with an ELISA reader at 570 nm.

Mechanism of Action Study. Hep3B cells (5.3×10^7) were treated with **3b** at different concentration or duration and then placed in 1 mL of the lysis buffer (10% glycerol, 1% Triton X-100, 137 mM NaCl, 10 mM NaF, 1 mM EGTA, 5 mM EDTA, 1 mM sodium pyrophosphate, 20 mM Tris-HCl, pH 7.9, 100 mM β-glycerophosphate, 1 mM sodium orthovanadate, 0.1% SDS, 10 μg/mL aprotinin, 1 mM phenylmethylsulfonyl fluoride, and 10 μg/mL leupeptin). The suspensions were centrifuged at 9000*g* for 1 min in a model 3200 Eppendorf/Brinkman centrifuge, and the supernatant fraction was subsequently centrifuged at 10000*g* for 60 min. Protein content was determined against a standardized control, using the Bio-Rad protein assay kit (Bio-Rad Laboratories).

Molecular Modeling Study. Molecular flexible docking was performed by Dock 5.1.[22] The Kollman partial charges were applied to protein models for force field calculation. Energy-optimized 3D coordinates and partial charges of small molecules were calculated by Marvin 5.2.2,[23] Balloon 0.6,[24] and OpenBabel 2.2.3.[25] There were 1000 orientations searched and 200 conformers generated per cycle identified in the Dock program. The docked conformers were then rescored by HotLig[26] to predicted protein−ligand binding modes. Protein structural superimposition was calculated and represented by Chimera 1.4.1.[27]

Enzyme Spectrum Screen Assay.[28] MDS PharmaServices performed this testing under standard protocols.

In Vivo Antitumor Activity Assay. The Hep-3B tumor cell line was purchased from American Type Culture Collection (ATCC HB-8064, human ovarian carcinoma cells). A culture medium of DMEM, 90%, and fetal bovine serum, 10%, supplemented with 1% penicillin−streptomycin was used. The tumor cells were incubated in an atmosphere containing 5% CO_2 at 37 °C.

Balb/c Nude mice used in this study were male, 4−6 weeks age, weighing 18−20 g and provided by National Animal Center. All animals were housed in individually ventilated cages racks (IVC Racks, 36 Mini Isolator system) under specific pathogen-free (SPF) conditions throughout the experiment. Each cage (26.7 cm length × 20.7 cm width × 14.0 cm height) was sterilized with autoclave and contained eight mice. The animals were maintained in a hygienic environment under controlled temperature (20−24 °C) and humidity (40%−70%) with a 12 h light/dark cycle. The animals were given free access to sterilized lab chow and sterilized distilled water ad libitum. All aspects of this work, i.e., housing, experimentation, and disposal of animals, were performed in general accordance with the Guide for the Care and Use of Laboratory Animals (National Academy Press, Washington, DC, 1996).

In the xenograft tumor model of human ovarian carcinoma cell lines (Hep-3B, ATCC HB-8064) in male Balb/c Nude mice, compound **15** at doses 7.5, 15, and 30 mg/kg (iv or po, q.d.) was administered 5 days per week for 4 consecutive weeks and ceased at day 28. The tumor size and body weight were monitored and recorded for 28 days. Human ovarian carcinoma cells (HEP-3B, ATCC HB-8064) with 2×10^6 cells in 0.1 mL were injected subcutaneously into the right flank of the mice. When the tumor growth reached > 100 mm^3 in volume (assumed as day 0), the tumor-bearing animals were assigned into several groups (eight animals in each group) for study.

The body weight and tumor size were measured and recorded every 7 days during the experiment period of 28 days. Tumor volume (mm^3) was estimated according to the formula of length × $(width)^2 \times 0.5$ in mm^3. Tumor growth inhibition was calculated as *T*/*C* (treatment/control) by the following formula: $T/C = (T_n - T_0)/(C_n - C_0) \times 100\%$ (T_0, tumor volume of treated group on day 0; T_n, tumor volume of treated group on day *n*; C_0, tumor volume of control group on day 0; C_n, tumor volume of control group on day *n*).

Acknowledgment. The investigation was supported by research grants from the National Science Council of the Republic of China awarded to S.-C.K. (NSC Grant 96-2323-B-039-001, NSC Grant 97-2323-B-039-001) and to L.-J.H. (NSC Grant 95-2320-B039-011-MY3). The work was also

supported by Grant CA17625-32 from the National Cancer Institute, NIH (K.-H.L.).

Supporting Information Available: Literature references for enzyme spectrum screen assays. This material is available free of charge via the Internet at http://pubs.acs.org.

References

(1) Kuo, S. C.; Lee, H. Z.; Juang, J. P.; Lin, Y. T.; Wu, T. S.; Chang, J. J.; Lednicer, D.; Paull, K. D.; Lin, C. M. Synthesis and cytotoxicity of 1,6,7,8-substituted-2-(4′-substituted phenyl)-4-quinolones and related compounds: identification as antimitotic agents interacting with tubulin. *J. Med. Chem.* **1993**, *36* (9), 1146–1156.

(2) Li, L.; Wang, H. K.; Kuo, S. C.; Wu, T. S.; Lednicer, D.; Lin, C. M.; Hamel, E.; Lee, K. H. Antitumor agents. 150. 2′,3′,4′,5′,5,6,7-Substituted 2-phenyl-4-quinolones and related compounds: their synthesis, cytotoxicity, and inhibition of tubulin polymerization. *J. Med. Chem.* **1994**, *37* (8), 1126–1135.

(3) Li, L.; Wang, H. K.; Kuo, S. C.; Wu, T. S.; Mauger, A.; Lin, C. M.; Hamel, E.; Lee, K. H. Antitumor agents. 155. Synthesis and biological evaluation of 3′,6,7-substituted 2-phenyl-4-quinolones as antimicrotubule agents. *J. Med. Chem.* **1994**, *37* (20), 3400–3407.

(4) Chou, L. C.; Chen, C. T.; Lee, J. C.; Way, T. D.; Huang, C. H.; Huang, S. M.; Teng, C. M.; Yamori, T.; Wu, T. S.; Sun, C. M.; Chien, D. S.; Qian, K.; Morris-Natschke, S. L.; Hamel, E.; Lee, K. H.; Huang, L. J.; Kuo, S. C. Synthesis and preclinical evaluations of 2-(2-fluorophenyl)-6,7-methylenedioxyquinolin-4-one monosodium phosphate (CHM-1−P-Na) as a potent antitumor agent. *J. Med. Chem.* **2010**, *53* (4), 1616–1626.

(5) Kuo, S. C.; Teng, C. M.; Lee, K. H.; Huang, L. J.; Chou, L. C.; Chang, C. S.; Sun, C. M.; Wu, T. S.; Pan, S. L.; Way, T. D.; Lee, J. C.; Chung, J. G.; Yang, J. S.; Chen, C. T.; Huang, C. C.; Huang, S. M. Novel Hydrophilic Derivatives of 2-Aryl-4-quinolones as Anticancer Agents. WO 2008/070176 A1 (PCT), 2008. [Patent Applied in Taiwan (96146890), U.S. (12/448088), Australia (2007328034), Canada (2670292), China (200780044796.9), EU (07853279.3), India (3052/EHENP/2009), Japan (2009-540310), Korea (10-2009-7014196), New Zealand (577130), Russian Fedeation (2009124622), South Africa (2009/03694).]

(6) Chang, Y. H.; Hsu, M. H.; Wang, S. H.; Huang, L. J.; Qian, K.; Morris-Natschke, S. L.; Hamel, E.; Kuo, S. C.; Lee, K. H. Design and synthesis of 2-(3-benzo[*b*]thienyl)-6,7-methylenedioxyquinolin-4-one analogs as potent antitumor agents that inhibit tubulin assembly. *J. Med. Chem.* **2009**, *52* (15), 4883–4891.

(7) Hagmann, W. K. The many roles for fluorine in medicinal chemistry. *J. Med. Chem.* **2008**, *51* (15), 4359–4369.

(8) Press, J. B.; Bandurco, V. T.; Wong, E. M.; Hajos, Z. G.; Kanojia, R. M.; Mallory, R. A.; Deegan, E. G.; McNally, J. J.; Roberts, J. R.; Cotter, M. L.; Graden, D. W.; Lloyd, J. R. Synthesis of 5,6-dimethoxyquinazolin-2(1*H*)-ones. *J. Heterocycl. Chem.* **1986**, *23*, 1821–1828.

(9) Bandurco, V. T.; Schwender, C. F.; Bell, S. C.; Combs, D. W.; Kanojia, R. M.; Levine, S. D.; Mulvey, D. M.; Appollina, M. A.; Reed, M. S.; Malloy, E. A.; Falotico, R.; Moore, J. B.; Tobia, A. J. *J. Med. Chem.* **1987**, *30*, 1421–1426.

(10) Mizuta, H..; Watanabe, S.; Sakurai, Y.; Nishiyama, K.; Furuta, T.; Kobayashi, Y.; Iwamura, M. Design, synthesis, photochemical properties and cytotoxic activities of water-soluble caged L-leucyl-L-leucine methyl esters that control apoptosis of immune cells. *Bioorg. Med. Chem.* **2002**, *10*, 675–683.

(11) Unpublished data.

(12) Riedemann, J.; Sohail, M.; Macaulay, V. M. Dual silencing of the EGF and type 1 IGF receptors suggests dominance of IGF signaling in human breast cancer cells. *Biochem. Biophys. Res. Commun.* **2007**, *355*, 700–706.

(13) Mayer, S. C.; Banker, A. L.; Boschelli, F.; Di, L.; Johnson, M.; Kenny, C. H.; Krishnamurthy, G.; Kutterer, K.; Moy, F.; Petusky, S.; Ravi, M.; Tkach, D.; Tsou, H. R.; Xu, W. Lead identification to generate isoquinolinedione inhibitors of insulin-like growth factor receptor (IGF-1R) for potential use in cancer treatment. *Bioorg. Med. Chem. Lett.* **2008**, *18*, 3641–3645.

(14) Wood, E. R.; Shewchuk, L.; Hassel, A.; Nichols, J.; Truesdale, A. T.; Smith, D.; Carter, H. L.; Weaver, K.; Barrett, G.; Leesnitzer, T.; Alvarez, E.; Bardera, A. I.; Alamillo, A.; Cantizani, J.; Martin, J.; Smith, G. K.; Jensen, D. E.; Xie, H.; Mook, R.; Kumar, R.; Kuntz, K. Discovery of an inhibitor of insulin-like growth factor 1 receptor activation: Implications for cellular potency and selectivity over insulin receptor. *Biochem. Pharmacol.* **2009**, *78* (12), 1438–1447.

(15) Favelyukis, S.; Till, J. H.; Hubbard, S. R.; Miller, W. T. Structure and autoregulation of the insulin-like growth factor 1 receptor kinase. *Nat. Struct. Biol.* **2001**, *8* (12), 1058–1163.

(16) Wu, J.; Li, W.; Craddock, B. P.; Foreman, K. W.; Mulvihill, M. J.; Ji, Q. S.; Miller, W. T.; Hubbard, S. R. Small-molecule inhibition and activation-loop trans-phosphorylation of the IGF1 receptor. *EMBO J.* **2008**, *27* (14), 1985–1994.

(17) Selga, E.; Oleaga, C.; Ramírez, S.; Almagro, M. C.; Noé, V.; Ciudad, C. J. Networking of differentially expressed genes in human cancer cells resistant to methotrexate. *Genome Med.* **2009**, *1* (9), 83.

(18) Paull, K. D.; Shoemaker, R. H.; Hodes, L.; Monks, A.; Scudiero, D. A.; Rubinstein, L.; Plowman, J.; Boyd, M. R. Display and analysis of patterns of differential activity of drugs against human tumor cell lines: development of mean graph and COMPARE algorithm. *J. Natl. Cancer Inst.* **1989**, *81* (14), 1088–1092.

(19) Monks, A.; Scudiero, D.; Skehan, P.; Shoemaker, R.; Paull, K.; Vistica, D.; Hose, C.; Langley, J.; Cronise, P.; Vaigro-Wolff, A.; Gray-Goodrich, M.; Campbell, H.; Mayo, J.; Boyd, M. Feasibility of a high-flux anticancer drug screen using a diverse panel of cultured human tumor cell lines. *J. Natl. Cancer Inst.* **1991**, *83*, 757–766.

(20) Chen, C. J.; Hsu, M. H.; Kuo, S. C.; Lai, Y. Y.; Chung, J. G.; Huang, L. J. (2*E*)-*N*,*N*-Dibutyl-3-(4-hydroxy-3-methoxyphenyl)-acrylamide induces apoptosis and cell cycle arrest in HL-60 cells. *Anticancer Res.* **2007**, *27*, 343–349.

(21) Hsu, M. H.; Chen, C. J.; Kuo, S. C.; Chung, J. G.; Lai, Y. Y.; Teng, C. M.; Pan, S. L.; Huang, L. J. 2-(3-Fluorophenyl)-6-methoxyl-4-oxo-1,4-dihydroquinoline- 3-carboxylic acid (YJC-1) induces mitotic phase arrest in A549 cells. *Eur. J. Pharmacol.* **2007**, *559*, 14–20.

(22) Kuntz, I. D.; Blaney, J. M.; Oatley, S. J.; Langridge, R. L. A geometric approach to macromolecule-ligand interactions. *J. Mol. Biol.* **1982**, *161*, 269–288.

(23) Marvin was used for drawing, displaying, and characterizing chemical structures, substructures and reactions. *Marvin*, version 5.2.2; ChemAxon: Budapest, Hungary, 2009; http://www.chemaxon.com.

(24) Vainio, M. J.; Johnson, M. S. Generating conformer ensembles using a multiobjective genetic algorithm. *J. Chem. Inf. Model.* **2007**, *47*, 2462–2474.

(25) Guha, R.; Howard, M. T.; Hutchison, G. R.; Murray-Rust, P.; Rzepa, H.; Steinbeck, C.; Wegner, J. K.; Willighagen, E. The blue obelisk. Interoperability in chemical informatics. *J. Chem. Inf. Model.* **2006**, *46* (3), 991–998.

(26) Wang, S. H., HotLig: A Molecular Surface-Directed Approach to Scoring Protein−Ligand Interactions. (Distributed by the author) Institute of Cellular and Organismic Biology: Academia Sinica, Taiwan, **2010**.

(27) Pettersen, E. F.; Goddard, T. D.; Huang, C. C.; Couch, G. S.; Greenblatt, D. M.; Meng, E. C.; Ferrin, T. E. UCSF Chimera, a visualization system for exploratory research and analysis. *J. Comput. Chem.* **2004**, *25*, 1605–1612.

(28) References are provided in Supporting Information.